


# Clamping force control based on dynamic model estimation for electromechanical brakes

Proc IMechE Part D:  
J Automobile Engineering  
2018, Vol. 232(14) 2000–2013  
© IMechE 2017  
Article reuse guidelines:  
sagepub.com/journals-permissions  
DOI: 10.1177/0954407017738394  
journals.sagepub.com/home/pid  


Giseo Park and Seibum B Choi

## Abstract

The electromechanical brake (EMB) is expected to be utilized for future brake systems due to its many advantages. In this paper, keeping commercialization of the EMB in mind, a new EMB clamping force controller is proposed to overcome the limitations of the existing controller, namely, the extra cost for sensor installation and response delay. To design the controller, both mechanical parts and electrical parts in the EMB have to be mathematically analyzed. Also, dynamic models, clamping force, and friction torque are estimated to generate some feed-forward terms of the controller. With an estimation of the contact point where brake pads start to come into contact with a disk wheel, the clamping force is expressed as a polynomial curve versus the motor angle. The estimated clamping force is evaluated in comparison with measured values by a load cell. The proposed controller is based on an adaptive sliding mode control method with an adaptive law reducing errors of the friction torque model. Lastly, the performance of the entire control system is compared with that of the existing controller on a test bench.

## Keywords

Electromechanical brake, estimation, clamping force, friction torque, adaptive sliding mode control

Date received: 29 March 2017; accepted: 28 September 2017

## Introduction

Influenced by technological advances, interest in brake-by-wire systems (BBWs) has increased steadily in the automotive industry. BBWs can provide both superior performance and convenience for drivers.<sup>1,2</sup> Electromechanical brake (EMB) systems are one kind of BBW that have replaced some of the complex hydraulic components of conventional braking systems with electrical components, such as a brake pedal sensor, a pedal simulator, and control units.<sup>3</sup> A brake command transmitted through these electrical components drives a motor, which generates brake torque. As brake pads vertically come into contact with a disk wheel on both sides, clamping force and braking torque are simultaneously generated.

The EMB has some advantages over conventional hydraulic brake systems, such as faster response for shorter braking distance, lighter weight, and better space efficiency.<sup>1</sup> Also it can be more easily connected to some vehicle chassis control systems, such as anti-lock braking systems (ABSs) and electronic stability control systems (ESCs).<sup>4,5</sup> These advantages have attracted many researchers and industry experts to

study EMBs for commercialization.<sup>1–10</sup> Some researchers have expected that EMBs can be utilized for the brake systems of future vehicles.<sup>1,3,6</sup> A vehicle equipped with an EMB must control it with high accuracy for implementation of high-level control systems, such as ABSs and ESCs.<sup>6</sup>

So far, most EMB systems have been controlled by a clamping force feedback controller, which has cascaded clamping force, motor velocity, and motor current control loops.<sup>7,8</sup> However, a load cell measuring the clamping force is too expensive to be installed in production vehicles and is not accurate at high temperatures.<sup>7</sup> So, the force feedback from the load cell has both robustness and reliability issues. To solve these problems, an effective method by which the clamping force is estimated without a load cell is required. Schwarz et al.<sup>9</sup> proposed a basic algorithm for clamping force

Department of Mechanical Engineering, KAIST, Republic of Korea

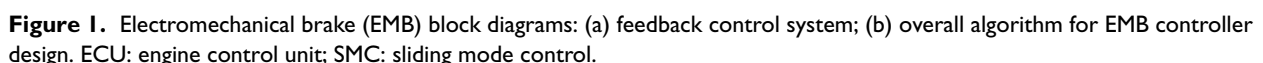
## Corresponding author:

Seibum B Choi, Department of Mechanical Engineering, KAIST, 291 Daehak-ro, Yuseong-gu, Daejeon 305-701, Republic of Korea.  
Email: sbchoi@kaist.ac.kr

Furthermore, the developed clamping force estimator can be utilized to design a new controller including some feed-forward terms related to the EMB dynamic models. It is anticipated that the newly proposed controller can avoid response phase lag occurring frequently in the existing controller. For this purpose, an estimation of the other dynamic model, friction torque, is essential. If these estimated dynamic models have acceptable differences in actual values, they can have a positive effect and improve control performances. An overall algorithm for EMB controller design is illustrated by the block diagrams in Figure 1(b). As shown in these diagrams, prior to completion of the controller design, the feedback control system is performed only

The remainder of this paper is organized as follows. Mathematical models of both electrical and mechanical parts are introduced in the second section. Estimation algorithms for the contact point, clamping force, and friction torque are developed in the third section. In the fourth section, the new clamping force controller, which uses the outcomes of the developed estimators, is presented with a formulation of the adaptive SMC method. Some experiments for verification of the new controller are performed on an EMB test bench and the results are analyzed in the fifth section. Finally, the sixth section concludes the paper.

Figure 2(a) illustrates the overall structure of an EMB composed of primary components such as a permanent magnet synchronous motor (PMSM). Some reduction gears and one planetary gear set reducing the angular velocity of the PMSM are connected to the PMSM in series. Then, this rotational motion is converted into the linear motion of the piston through the ball screw.



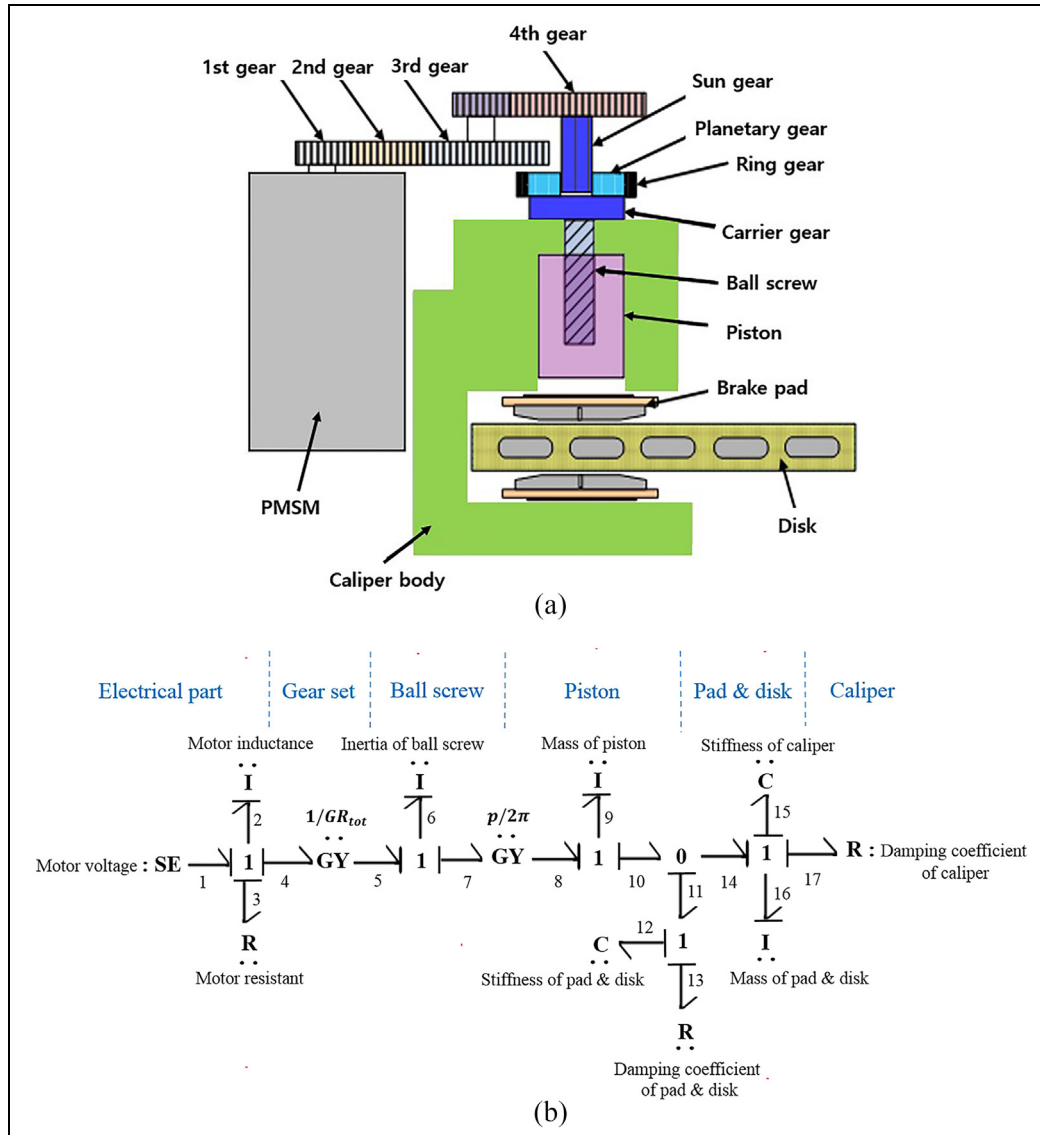


**Figure 2.** Electromechanical brake structure: (a) block diagram; (b) bond graph. PMSM: permanent magnet synchronous motor.

While the linear motion presses the disk between two pads, the outer caliper body clamps the disk at the same time. The stiffness of this caliper body accounts for the main portion of overall brake stiffness.<sup>9</sup> Modeling of the EMB is simply divided into the electrical and mechanical parts. Also, the EMB structure can be expressed as a bond graph, as shown in Figure 2(b): the bond graph theory is well explained by Ma et al.<sup>12</sup>

### Modeling of the electrical part

The PMSM is suitable to control the EMB due to its high precision in both angular velocity and motor current control.<sup>13,14</sup> In the PMSM, three-phase vectors of a voltage or a current are transformed to two-phase vectors, which are represented with stator orthogonal coordinates, the  $\alpha - \beta$  axis.<sup>15</sup> This is called the Clarke transform

$$\begin{bmatrix} f_\alpha \\ f_\beta \end{bmatrix} = \begin{bmatrix} 1 & -\frac{1}{2} & -\frac{1}{2} \\ 0 & \frac{\sqrt{3}}{2} & -\frac{\sqrt{3}}{2} \end{bmatrix} \begin{bmatrix} f_a \\ f_b \\ f_c \end{bmatrix} \quad (1)$$

Here,  $f$  is the voltage or the current. Subsequently, the Park transform is performed to convert these stator orthogonal coordinates into others, the  $d - q$  axis, which rotates synchronously with the rotor.<sup>13-16</sup> The formula of the Park transform is expressed as follows

$$\begin{bmatrix} f_d \\ f_q \end{bmatrix} = \begin{bmatrix} \cos \theta_s & \sin \theta_s \\ -\sin \theta_s & \cos \theta_s \end{bmatrix} \begin{bmatrix} f_\alpha \\ f_\beta \end{bmatrix} \quad (2)$$

where  $\theta_s$  is the electrical rotor angle. Voltage equations with  $d$  and  $q$  axes are described in following equations<sup>1,13-17</sup>

$$v_d = Ri_d + L_d \frac{di_d}{dt} - \omega_s L_q i_q \quad (3)$$

$$v_q = Ri_q + L_q \frac{di_q}{dt} + w_s(L_d i_d + \psi_{af}) \quad (4)$$

$$w_s = n_p w_m \quad (5)$$

where  $v_d$  and  $v_q$  are the voltages;  $i_d$ ,  $i_q$  are the currents;  $L_d$ ,  $L_q$  are the inductances of each axis;  $w_m$ ,  $w_s$  are the mechanical and electrical angular velocity, respectively;  $R$  is the stator resistance;  $\psi_{af}$  is the flux linkage; and is  $n_p$  the number of pole pairs. The torque of the interior permanent magnet synchronous motor (IPMSM) used in this research is given as

$$T_m = \frac{3}{2} n_p [\psi_{af} i_q + (L_d - L_q) i_d i_q] \quad (6)$$

To generate maximum motor torque, the IPMSM is controlled such that  $i_d$  becomes zero.<sup>13–16</sup> Therefore, the motor torque, which is linearly proportional to the motor current, can be simply expressed as direct current (DC) motor torque as follows

$$T_m = \frac{3}{2} n_p \psi_{af} i_q = K_m i_q \quad (7)$$

where  $K_m$  represents the motor torque constant.

### Modeling of the mechanical part

The motor angular velocity is reduced by passing through a series of reduction gears and the planetary gear set. The relations between two gears connected to each other are described as

$$\begin{aligned} w_1 &= w_m \\ w_2 &= w_1 / (s_1 \times GR_1) \\ w_3 &= w_2 / (s_2 \times GR_2) \\ w_4 &= w_3 / (s_3 \times GR_3) \\ w_{carrier} &= w_4 / (s_4 \times GR_{planetary}) \end{aligned} \quad (8)$$

where  $GR$  and  $s$  are the gear ratio and the gear efficiency, respectively. Also, each subscript in equation (8) denotes the number of each gear in Figure 2(a). Then, the rotational motion of the carrier gear is converted into the linear motion of the ball screw. Eventually, the displacement of the ball screw is linearly proportional to the motor angle.<sup>5,9</sup> It is described as

$$x_{screw} = \frac{1}{GR_{tot}} \frac{p}{2\pi} \theta_m = k_{screw} \theta_m \quad (9)$$

where

$$\begin{aligned} GR_{tot} &= s_{tot} \times GR_1 \times GR_2 \times GR_3 \times GR_{planetary} \\ s_{tot} &= s_1 \times s_2 \times s_3 \times s_4. \end{aligned}$$

Here,  $GR_{tot}$  is the total gear ratio of all rotational parts, which is calculated by the multiplication of all gear ratios. Also,  $s_{tot}$  denotes the total gear efficiency. Then,  $p$  and  $k_{screw}$  are the pitch of the ball screw and translating gain, respectively.  $J_{tot}$ , the total inertia of the system from the perspective view of the motor angle, is expressed as

$$\begin{aligned} J_{tot} &= J_{motor} + J_{GR1} + \frac{J_{GR2}}{(s_1 \times GR_1)^2} \\ &+ J_{GR3} / (s_1 \times s_2 \times GR_1 \times GR_2)^2 \\ &+ \{J_{GR4} + (J_{planetary} + J_{screw}) / (s_4 \times GR_{planetary})^2\} / \\ & (s_1 \times s_2 \times s_3 \times GR_1 \times GR_2 \times GR_3)^2 \end{aligned} \quad (10)$$

where each subscript of  $J$  corresponds to each rotational component. The motor torque in Equation (7) is equal to the sum of  $T_L$ , the load torque;  $T_i$ , the inertia torque that is proportional to the motor angular acceleration with the total inertia in equation (10); and  $T_f$ , the friction torque<sup>3,5–10</sup>

$$T_L = \frac{k_{screw}}{s_s} F_{cl} = k_{cl} F_{cl} \quad (11)$$

$$T_m = T_L + J_{tot} \frac{d^2 \theta_m}{dt^2} + T_f \quad (12)$$

where

$$T_f(\theta_m) = \text{sgn}(w_m)(\gamma F_{cl} + T_{f0}).$$

Here,  $s_s$  and  $k_{cl}$  are the efficiency of the ball screw and the gearing gain, respectively. Also,  $\gamma$  and  $T_{f0}$  are the coefficient of Coulomb friction and the offset term, respectively.<sup>6</sup>

### Dynamic model estimation

Knowing the dynamic models, such as the clamping force and friction torque, is very valuable for controlling the EMB. However, as mentioned in the first section, using a load cell to measure the clamping force is not recommended due to extra cost and problems associated with installation.<sup>1,3,5</sup> Also, directly measuring the friction torque with any production sensor is impossible. Instead, both  $F_{cl}$  and  $T_f$  can be described as functions of the motor angle.<sup>9</sup> Thus, based on only one degree of freedom  $\theta_m$ , the new EMB controller in the fourth section can be easily controlled.

### Contact point estimation

Estimation of the contact point takes priority over clamping force estimation. In developing an algorithm for contact point estimation, both the motor current and the motor angle are individually measured by corresponding sensors during the special brake operation, as shown in Figure 3. This brake operation is divided into pressing and releasing the brake pedal, which means moving the EMB ball screw forward and backward, respectively. In particular, when a car is started, this operation can be quickly performed. Many kinds of vehicle are equipped with a shift-lock system that prevents a driver from starting a vehicle without using the brake.<sup>18</sup> Thus, most drivers can naturally implement the brake operation during starting a vehicle.

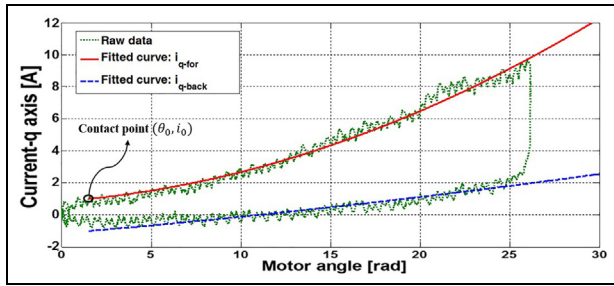


Figure 3. Curve fitting with the contact point.

In Figure 3, when the motor current becomes greater than the constant threshold  $i_0$ , the motor angle at that time can be regarded as the contact point  $\theta_0$ .<sup>19</sup> During the forward operation that makes the ball screw move forward, the polynomial curve on the basis of the relation between  $i_q$  and  $\theta_m$  starting at  $\theta_0$  is described as follows

$$i_{q-for}(\theta_m) = \alpha_{for}(\theta_m - \theta_0)^2 + \beta_{for}(\theta_m - \theta_0) + i_0 \quad (13)$$

A recursive least square (RLS) method used for every curve fitting in this paper is introduced in the following explanation. The RLS method has some advantages, such as much faster convergence and less computation than those of the least square method. It is suitable for a particular curve fitting that is desired to be completed quickly. The basic idea of the RLS method is to find an estimated parameter  $\hat{w}$ , which makes the sum of the squares of the error between approximated data  $\phi^T(i)\hat{w}$  and measured data  $y(i)$  minimal.<sup>17</sup> This sum, the cost function  $V(\hat{w}, k)$ , is defined as follows

$$V(\hat{w}, k) = \frac{1}{2} \sum_{i=1}^k \lambda^{k-i} (y(i) - \phi^T(i)\hat{w})^2 \quad (14)$$

where  $k$  denotes the number of samples. In the case of equation (13),  $y(i)$  is the motor current  $i_q - i_0$  and  $\phi^T(i)$  the motor angle  $\theta_m - \theta_0$  at the  $i$ th sample in the forward operation. Also,  $\hat{w}$  denotes the coefficients of the second-order polynomial curve  $\alpha_{for}$  and  $\beta_{for}$ . To find optimal  $\hat{w}$ ,  $V(\hat{w}, k)$  is differentiated by  $\hat{w}$ . Consequently, the following forms are derived<sup>20,21</sup>

$$\hat{w}(k) = \hat{w}(k-1) + L(k)\{y(k) - \phi^T(k)\hat{w}(k-1)\} \quad (15)$$

where

$$\begin{aligned} L(k) &= P(k)\phi(k) \\ &= P(k-1)\phi(k)\{\lambda_f + \phi^T(k)P(k-1)\phi(k)\}^{-1} \\ P(k) &= \{I - L(k)\phi^T(k)\}\lambda_f^{-1}P(k-1) \\ &= \frac{1}{\lambda_f}\{P(k-1) - \frac{P(k-1)\phi(k)\phi^T(k)P(k-1)}{\lambda_f + \phi^T(k)P(k-1)\phi(k)}\} \end{aligned}$$

Here,  $L(k)$  and  $P(k)$  are the update gain and the error covariance matrix, respectively, and  $\lambda_f$  is the forgetting factor. It determines the weighting of the

Table 1. The root mean square (RMS) errors of polynomial curve fitting.

Order of a polynomial	RMS error (N)
1	754.9381
2	110.0949
3	110.0933
4	110.0930
5	110.0956
8	110.0968

influence of old samples, which are not strongly related to newly estimated  $\hat{w}(k)$ . In the calculation of  $\hat{w}(k)$ , the smaller  $\lambda_f$  is, the greater the influence of the comparatively recent sample is. Generally, the value of  $\lambda_f$  is chosen in the interval  $[0.9, 1]$ .<sup>20</sup>

### Clamping force estimation

Assuming that both the backlash of the gears and elastic hysteresis of the brake pads are negligible, the relationship between  $F_{cl}$  and  $\theta_m$  can be expressed as a polynomial with no hysteresis.<sup>3,9,10</sup> The polynomial function is an appropriate mathematical model for the relationship.

From the preceding analysis in Table 1 showing the RMS errors between the actual and estimated clamping forces, a second-order polynomial is considered an optimum. In Figure 3, during the backward operation, the motor current  $i_{q-back}$  can be expressed as a second-order polynomial as in equation (13). It is described as

$$i_{q-back}(\theta_m) = \alpha_{back}(\theta_m - \theta_0)^2 + \beta_{back}(\theta_m - \theta_0) - i_0 \quad (16)$$

To find  $\alpha_{back}$  and  $\beta_{back}$ , the raw data  $i_{q-back} + i_0$  and  $\theta_m - \theta_0$  are utilized to perform the RLS method in the same way as equations (13)–(15). Depending on the direction of each brake operation, the clamping force can be defined from the torque balance equation (12)

$$\begin{aligned} \text{Forward: } F_{cl} &= \frac{1}{k_{cl}}(K_m i_{q-for} - J_{tot} \frac{d^2 \theta_{m-for}}{dt^2} + T_f) \\ \text{Backward: } F_{cl} &= \frac{1}{k_{cl}}(K_m i_{q-back} - J_{tot} \frac{d^2 \theta_{m-back}}{dt^2} - T_f) \end{aligned} \quad (17)$$

Generally,  $T_f$  in the EMB is regarded as a Coulomb friction torque, whose sign is changed according to each brake operation.<sup>3,9,22,23</sup> When the motor angle is the same, it is reasonable to assume that the absolute value of the friction torque is the same regardless of the direction of the brake operation. Schwarz et al.<sup>9</sup> proposed that the friction torque can be cancelled out due to this characteristic. Equations (13) and (16) can be used to substitute for  $i_{q-for}$  and  $i_{q-back}$  in equation (17), respectively. As shown in Figure 4(a), clamping force is



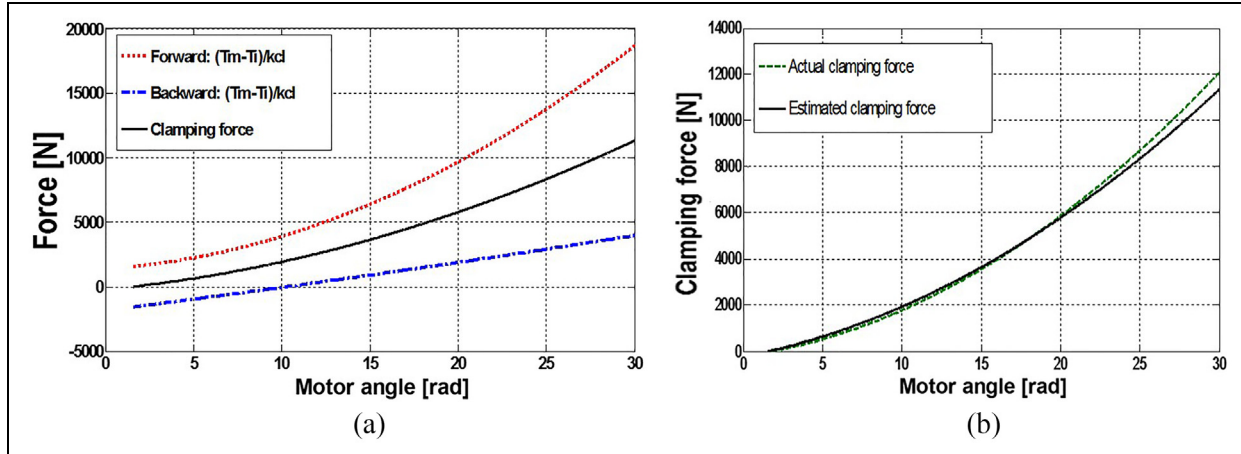


**Figure 4.** Characteristic curve fitting: (a) estimated clamping force versus the motor angle; (b) comparison with the actual clamping force.

**Table 2.** The specifications of a midsize vehicle (LF Sonata).

Parameter	Quantity	Value
$m$	Vehicle mass + people	1560 kg
$r_f$	Effective radius of the front disc	130.9 mm
$\mu_f$	Nominal pad friction coefficient at the front brake pad	0.38
$r_r$	Effective radius of the rear disc	124.0 mm
$\mu_r$	Nominal pad friction coefficient at the rear brake pad	0.38
$R_w$	Effective rolling radius of tire	330 mm

estimated by taking the average of the formulas in Equation (17) over the whole range of the motor angle. The signal noises of  $d^2\theta_m/dt^2$  are removed by utilizing the low pass filter

$$\hat{F}_{cl} = \frac{K_m}{2k_{cl}}(i_{q-for} + i_{q-back}) - \frac{J_{tot}}{2k_{cl}} \frac{d^2}{dt^2}(\theta_{m-for} + \theta_{m-back}) \quad (18)$$

Lastly, by using the RLS method again, this estimated clamping force can be expressed as a polynomial function of the motor angle. The function starting at the contact point is described as

$$\hat{F}_{cl-fitting}(\theta_m) = K_2(\theta_m - \theta_0)^2 + K_1(\theta_m - \theta_0) \quad (19)$$

where  $K_2$  and  $K_1$  are coefficients calculated by the RLS method. Figure 4(b) compares the actual and estimated clamping force versus the motor angle; its range up to 30 rad is a primary operational range for a midsize vehicle (Hyundai LF Sonata). The estimated curve is quite close to the actual curve, which is based on measured values by a load cell.

To verify the accuracy of the estimation, an appraisal standard is set up in this study. Firstly, it is assumed that EMBs are installed in all wheels of the midsize vehicle (see the specifications in Table 2). Also, only longitudinal motion of vehicle is considered. The brake torques of the front and rear wheels are as follows

$$\begin{aligned} \text{Front wheel : } T_{b,f} &= 2\mu_f r_f F_{cl} \\ \text{Rear wheel : } T_{b,r} &= 2\mu_r r_r F_{cl} \end{aligned} \quad (20)$$

The dynamic equation of the vehicle wheel in the braking situation is represented as follows

$$\begin{aligned} J_w \dot{\omega} &= R_w F_x - T_b \\ F_x &\approx \frac{T_b}{R_w} (T_b \gg J_w \dot{\omega}) \end{aligned} \quad (21)$$

From the sum of tire longitudinal forces, the clamping force can be derived as a function of vehicle longitudinal acceleration  $a_x$ . It is assumed that  $F_{cl}$  in every wheel is the same

$$\begin{aligned} \sum_{i=1}^4 F_{x,i} &= \frac{2(T_{b,f} + T_{b,r})}{R_w} = ma_x \\ \therefore F_{cl} &= \frac{R_w ma_x}{4(\mu_f r_f + \mu_r r_r)} \end{aligned} \quad (22)$$

A low deceleration of less than 0.03g in a vehicle represents smooth and comfortable riding performance that is difficult to notice by a driver.<sup>24</sup> From equation (22), the clamping force of approximately 0.39 kN to each wheel is required to decelerate the midsize vehicle to 0.03g. So, the error tolerance of clamping force estimation or control in this paper is set to 0.39 kN. As the results in Figure 5(a) show, with a full pad thickness of

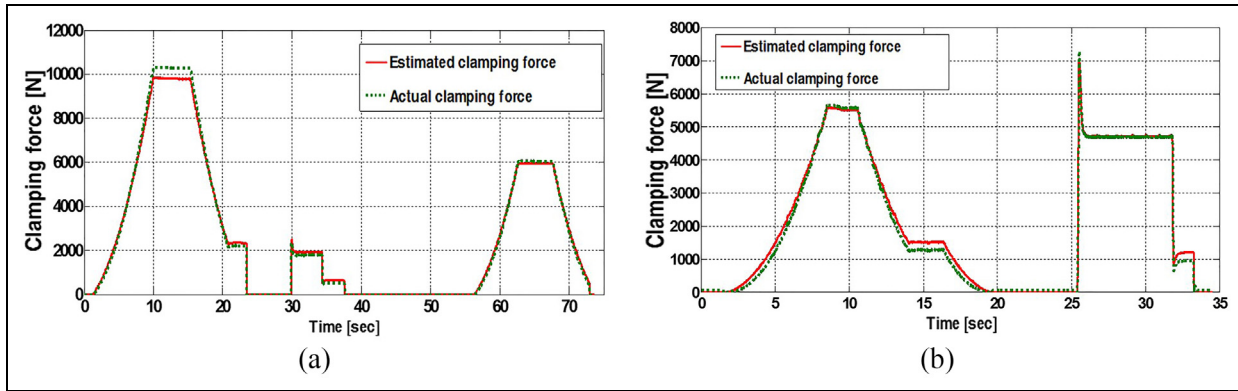


**Figure 5.** Clamping force estimation: (a) with 13 mm pad thickness; (b) with 6 mm pad thickness.

13 mm, the maximum error is less than 0.39 kN. Even when the pad thickness decreases to 6 mm due to pad wear, the accuracy is still maintained in that range, as seen in Figure 5(b). Therefore, according to these results, the estimated clamping force including the contact point estimation presented in the *Contact point estimation* section is suitable to be part of the new clamping force controller. Also, to manage the change of the pad thickness, the curve fitting process (equations (13)–(19)) is desired to be periodically performed.

### Friction torque estimation

On the surfaces of some components, such as the motor, the gears, and the ball screw, a lumped friction torque resisting the external torque  $T_E (= T_m - T_L)$  is generated synthetically. In some previous papers,<sup>3,9</sup> the kinetic friction torque during slipping motions of all rotational components is expressed as a function of the clamping force (refer to  $T_f(\theta_m)$  in equation (12)). In this paper, for elaborate modeling, the load dependency of friction torque is newly expressed as a second-order polynomial function of the motor angle

$$T_f(\theta_m) = \begin{cases} \text{sgn}(w_m)\{f_2(\theta_m - \theta_0)^2 + f_1(\theta_m - \theta_0) + T_{f0}\} & \text{if } \theta_m \geq \theta_0 \\ T_{f0}\text{sgn}(w_m) & \text{else} \end{cases} \quad (23)$$

Here,  $f_1$  and  $f_2$  are the load-dependent coefficients and  $T_{f0}$  is the offset term.

After many brake maneuvers, the brake pad can be over heated and the heat of the pad is concurrently propagated into the nearby components.<sup>9,25</sup> This remarkable change of temperature is the main parameter affecting the change of friction in an EMB actuator. Therefore, although nominal values of  $f_1$ ,  $f_2$ , and  $T_{f0}$  in equation (23) are given at the beginning, they are desired to be updated to enhance the robustness. Here  $\hat{\eta}$  is defined as a varying scale of load term  $f_2(\theta_m - \theta_0)^2 + f_1(\theta_m - \theta_0)$  (initial  $\hat{\eta} = 1$ ) and, then, the

nominal  $T_f(\theta_m)$  can be adaptively changed by the variable  $\hat{\eta}$ . While the estimated  $\hat{\eta}$  converges to real  $\eta$  by an adaptation law, the error of friction torque  $\tilde{T}_f(\theta_m)$  is reduced.<sup>26</sup> The adaptation law is introduced in the next section.

### Controller design

Generally, a brake actuator should have a fast response without time delay. The faster the reaction of the motor angle control in the EMB, the faster the generation of the clamping force is, and the shorter the braking distance is. In this section, a controller is proposed that is based on the clamping force and friction torque estimators in the third section. The block diagram of the control scheme is as shown in Figure 6.

Based on the inverse of equation (19), the desired clamping force  $F_{cl-des}$  can be converted to the desired motor angle  $\theta_{m-des}$ . Since equation (19) is a strictly increasing function, each value of  $F_{cl-des}(\geq 0)$  is matched one-to-one with the corresponding  $\theta_{m-des}(\geq \theta_0)$

$$\theta_{m-des} = (-K_1 + \sqrt{K_1^2 + 4K_2 F_{cl-des}})/2K_2 + \theta_0 \quad (24)$$

To determine the control input, the adaptive SMC method is used. Firstly, the torque balance equation (12) is rearranged as the following formula for the angular acceleration

$$\ddot{\theta}_m = (K_m i_q - k_{cl} F_{cl} - T_f)/J_{tot} \quad (25)$$

The tracking error  $e$  and variable  $s$ , which are bounded physically, are separately defined as

$$\begin{aligned} e &= \theta_m - \theta_{m-des} \\ s &= \dot{e} + \lambda e \end{aligned} \quad (26)$$

where the positive constant  $\lambda$  is the only tuning parameter. Let  $\text{sat}$  be the saturation function of  $s$ : set  $\text{sat}(x) = x/\varepsilon$  as  $|x| \leq \varepsilon$  and  $\text{sat}(x) = \text{sgn}(x)$  as  $|x| > \varepsilon$  where  $\varepsilon$  is a very small parameter

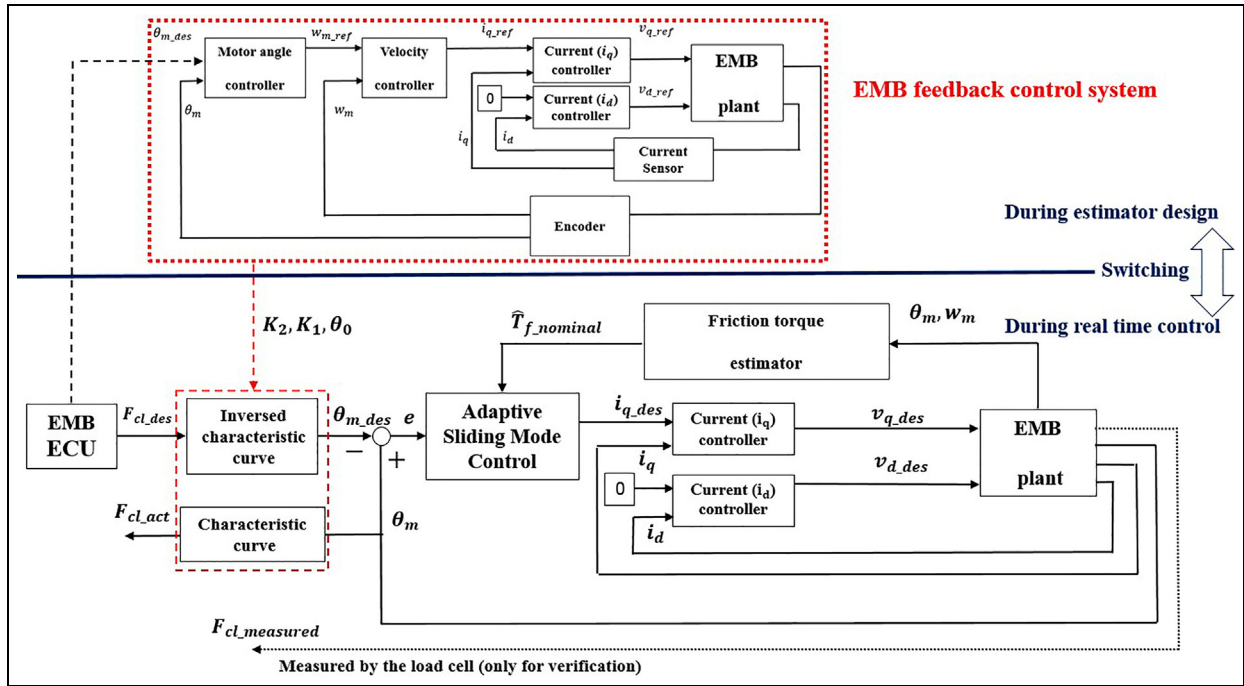


**Figure 6.** Block diagram of the proposed electromechanical brake (EMB) controller. ECU: engine control unit.

$$\dot{s} = -\lambda_{sat}(s) \quad (27)$$

The time derivative of  $s$  is written as

$$\dot{s} = \ddot{e} + \lambda \dot{e} = \ddot{\theta}_m - \ddot{\theta}_{m-des} + \lambda \dot{e} \quad (28)$$

The error dynamics can be written by substituting equation (28) into equation (27)

$$\ddot{\theta}_m - \ddot{\theta}_{m-des} + \lambda \dot{e} + \lambda sat(s) = 0 \quad (29)$$

Substituting equation (25) into  $\ddot{\theta}_m$  yields

$$(K_m i_q - k_{cl} F_{cl} - T_f) / J_{tot} - \ddot{\theta}_{m-des} + \lambda \dot{e} + \lambda sat(s) = 0 \quad (30)$$

Lastly,  $F_{cl}$  and  $T_f$  can be replaced with equations (19) and (23), respectively. At this point, it is assumed that the estimated  $F_{cl}$  is actual. Therefore, the motor current in equation (30) is regarded as the control input  $i_{q-des}$ , which is designed as

$$i_{q-des} = \frac{1}{K_m}(k_{cl}F_{cl} + \hat{T}_f + J_{tot}\ddot{\theta}_{m-des}) - \frac{\lambda J_{tot}}{K_m}(\dot{e} + \text{sat}(\dot{e} + \lambda e)) \quad (31)$$

where

$$\hat{T}_f = T_{f0} \text{sgn}(w_m) + \hat{\eta}(f_2(\theta_m - \theta_0)^2 + f_1(\theta_m - \theta_0)) \text{sgn}(w_m).$$

Here, equation (31) is the reference of the inner loop current PI feedback controller (see Figure 6). To prove the stability of the proposed algorithm by using Barbalat's lemma, consider a Lyapunov function candidate  $V$  that is lower bounded ( $V > 0$ ) and positive definite

$$V = \frac{1}{2}s^2 + \frac{1}{2k_a}\tilde{\eta}^2 \quad (32)$$

where

$$\tilde{\eta} = \eta - \hat{\eta}.$$

Here,  $k_a$  is a positive constant adaptation gain. Assuming that the real  $\eta$  varies slowly, the time derivative of  $V$  is obtained as

$$\begin{aligned}\dot{V} &= \dot{s}s + \frac{1}{k_a} \tilde{\eta}(\dot{\eta} - \dot{\hat{\eta}}) \\ &= ((K_m i_q - k_{cl} F_{cl} - T_f)/J_{tot} - \ddot{\theta}_{m-des} + \lambda \dot{e})s - \frac{1}{k_a} \tilde{\eta} \dot{\hat{\eta}}\end{aligned}\quad (33)$$

By substituting equation (31) into  $i_q$ ,  $\dot{s}$  and  $\dot{V}$  can be rewritten as

$$\begin{aligned}\dot{s} &= \frac{-\tilde{\gamma} \text{sgn}(w_m)(f_2(\theta_m - \theta_0)^2 + f_1(\theta_m - \theta_0)) - \lambda \text{sat}(s)}{J_{tot}} \\ \dot{V} &= -\frac{\lambda s \text{sat}(s)}{J_{tot}} \\ &\quad - \tilde{\eta} \left( \frac{\dot{\tilde{\eta}}}{k_a} + \frac{\text{sgn}(w_m)(f_2(\theta_m - \theta_0)^2 + f_1(\theta_m - \theta_0))}{J_{tot}} s \right)\end{aligned}\quad (34)$$

The adaptive law can be naturally obtained as follows

$$\dot{\hat{\eta}} = -k_a \text{sgn}(w_m)(f_2(\theta_m - \theta_0)^2 + f_1(\theta_m - \theta_0))s/J_{tot} \quad (35)$$

Hence,  $\dot{V}$  in equation (34) can be expressed as negative semidefinite, that is



**Table 3.** The main parameters of the electromechanical brake.

Symbol	Parameter	Value
$\psi_{af}$	Flux linkage	0.00402 Wb
$L_d$	Motor inductance ( <i>d</i> -axis)	78.8 $\mu$ H
$L_q$	Motor inductance ( <i>q</i> -axis)	93.5 $\mu$ H
$R$	Motor resistance	0.137 m $\Omega$
$K_m$	Motor torque constant	0.047 Nm/A
$n_p$	Number of pole pairs	3
$J_{tot}$	Total inertia moment	$3.184 \times 10^{-5}$ kg $\cdot$ m <sup>2</sup>
$GR_{tot}$	Total gear ratio	39:1
$p$	Pitch of ball screw	5 mm
$s_s$	Efficiency of ball screw	68%

$$\dot{V} = -\lambda s \text{sat}(s)/J_{tot} \leq 0 \quad (36)$$

From the following equation (37), it is verified that  $\ddot{V}$  is uniformly continuous in time

$$\ddot{V} = \lambda^2 (\text{sat}(s))^2 / J_{tot} \quad (37)$$

From equations (32)–(37), it is verified by using Barbalat's lemma that  $s \rightarrow 0$  as  $t \rightarrow \infty$ .<sup>26,27</sup> This implies that the tracking error  $e$  in equation (26) converges to zero. Also, since both  $s$  and  $\dot{s}$  converge to 0,  $\tilde{\eta}$  converges to 0 (refer to equation (34)).

Since the perfect clamping force estimation without the load cell is quite difficult, the modeling error  $\tilde{F}_{cl}$  is inevitable in the experimental results. However, it is expected that a sufficiently large gain  $\lambda$  can cancel out this modeling error.

## Experiments

### Experimental set-up

All experiments in this paper are performed using an EMB test bench (see Figure 7). All of the data are communicated by a controller area network (CAN). Figure 7(b) illustrates how the desired commands  $F_{cl-des}$  and  $\theta_{m-des}$  from the control desk are transmitted to the EMB plant. Also, the transmission of data from the EMB plant is shown;  $\theta_m$  and  $w_m$  are measured by an encoder, while  $i_a$ ,  $i_b$ , and  $i_c$  are measured by current sensors. Using a Micro-Autobox, all of the processes are monitored at a 1 ms sampling rate.<sup>28</sup> The feedback control system in Figure 1(a) for developing the estimators is downloaded onto the EMB engine control unit (ECU) through USB Multilink. The outer control loop consisting of the inversed characteristic curve, friction torque estimator, and the adaptive SMC is built in Micro-Autobox (see Figure 6). Thus, the control input is calculated in Micro-Autobox and is transmitted to the motor current feedback controller downloaded onto the EMB ECU. The system parameters are presented in Table 3.

### Experimental results

The controller design in the fourth section is evaluated in this section. First of all, an experiment with the feed-

forward control input  $i_{q-ff}$  only, that is, with a zero feedback gain ( $\lambda = 0$ ) in equation (31) and no adaptation law in equation (35), is performed.

The results of this experiment with the feed-forward control are shown in Figure 8. The clamping force command is applied as a step input (see Figure 8(b)). As shown in Figure 8(a), to follow this desired command  $F_{cl-des}$ ,  $i_{q-des}$  is calculated by the sum of the terms reflecting each dynamic model: the load torque, friction torque, and the inertia torque. The measured clamping force  $F_{cl-measured}$  obtained from the load cell and actual clamping force  $F_{cl-act}$  (the output of the controller) are simultaneously generated (see Figure 6).  $F_{cl-measured}$  from a load cell is for the purpose of monitoring only and are not used for the controls: if the clamping force estimation is perfect,  $F_{cl-act}$  will be equal to  $F_{cl-measured}$ .  $F_{cl-act}$  quickly reacts to the desired commands and promptly follows them. These results confirm the contribution of the feed-forward terms for the control performance improvement.

To validate the performance of the entire controller proposed in Figure 6, some experiments with various clamping force commands are performed. The step commands with various magnitudes, the triangular command, and sinusoidal command are individually applied into the proposed controller (see Figure 9). Regardless of the command, the acceptable control errors are shown. As well as the tracking errors between the desired and actual, those between the desired and measured are under the error tolerance of 0.39 kN. As a result, it is confirmed that the proposed controller based on dynamic model estimation can be applied to the various braking situations.

From the previous research, the adaptive law has the following characteristics<sup>26</sup>: (a) it increases the total system order; (b) due to the model error and signal noise, it may cause the instability of system. Therefore, the adaptive law in equation (35) is activated only when the steady-state error between the desired and actual is large. In Figures 9, 12(b), and 13(a), since each control result has an acceptable steady-state error, the adaptive laws are deactivated. This implies that the friction torque models are well estimated ( $\hat{\eta} = 1$ ,  $\eta \approx 1$ ).

To validate the performance of the adaptive law, the initial scale is intentionally set to an incorrect value, and the real scale is approximately 1 ( $\hat{\eta} = 0.57$ ,  $\eta \approx 1$ ). As shown in Figure 10, the adaptation law is activated by the large error between desired and actual clamping forces in about 3 s. It is confirmed that the control error in Figure 10(a) converges to 0, as the estimated parameter converges to the real scale in Figure 10(b).

Schwarz et al.<sup>2</sup> suggested a typical EMB clamping force controller, which was based on feedback errors with proportional (P) and integral (I) gains (see Figure 11). Figure 12 compares the performance of the proposed controller with that of the existing controller for the same step input of 8 kN. While the existing controller records the settling time within 2% error of 0.395 s, the proposed controller records 0.175 s. As shown in Figure 12(a), a

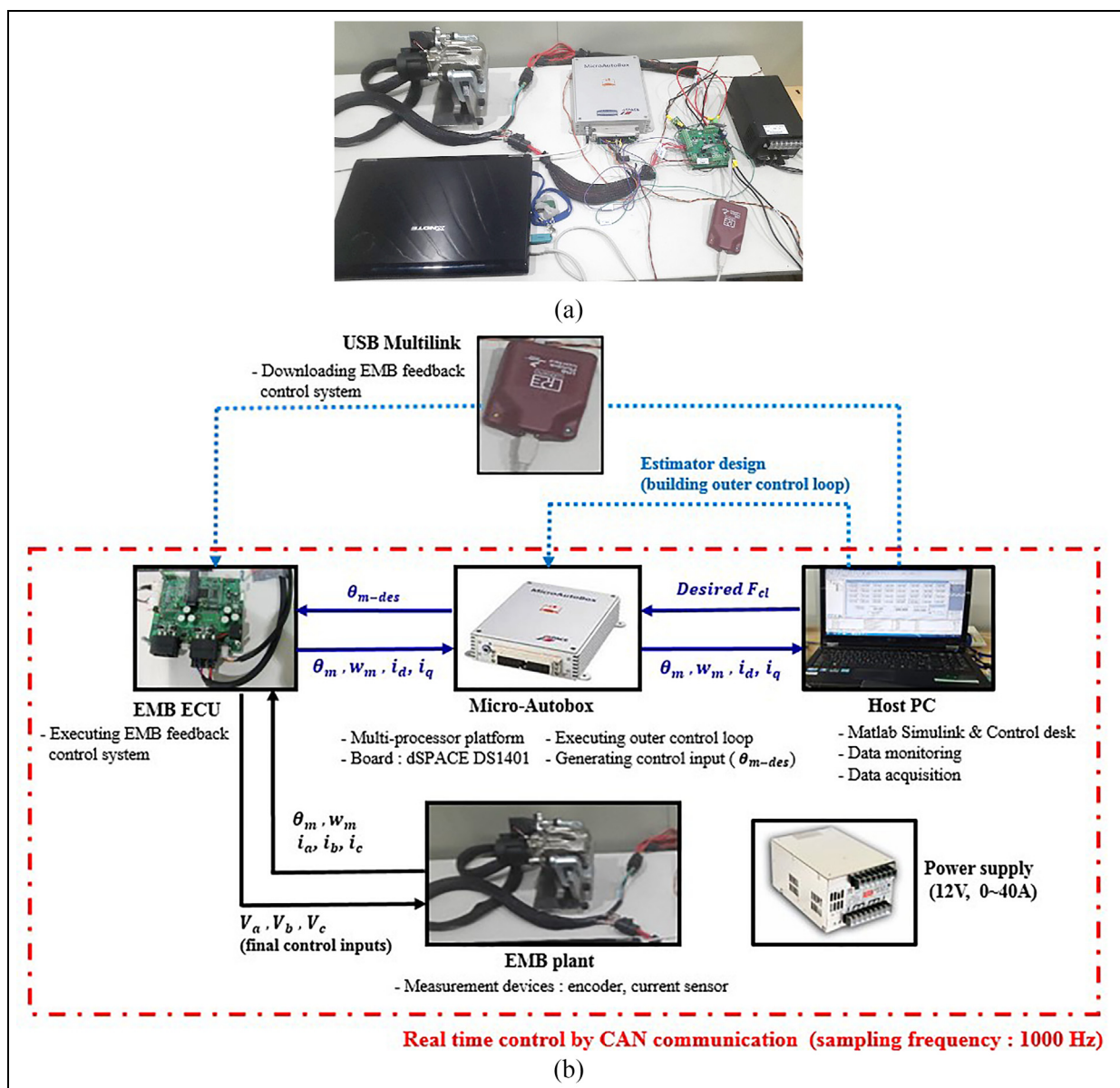


**Figure 7.** Electromechanical brake (EMB) test bench: (a) all equipments; (b) block diagram. ECU: engine control unit; CAN: controller area network.

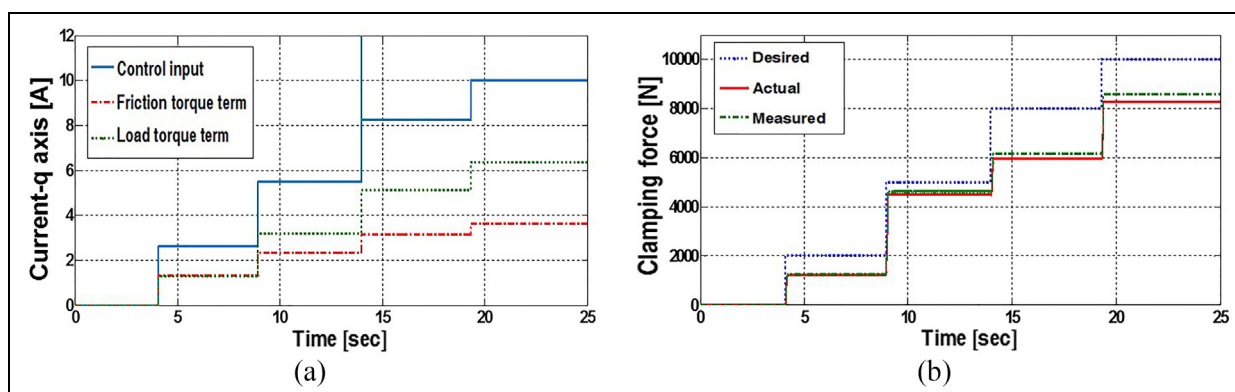


**Figure 8.** Only feed-forward control without feedback and adaptation: (a) control input; (b) the desired, actual, and measured clamping force.

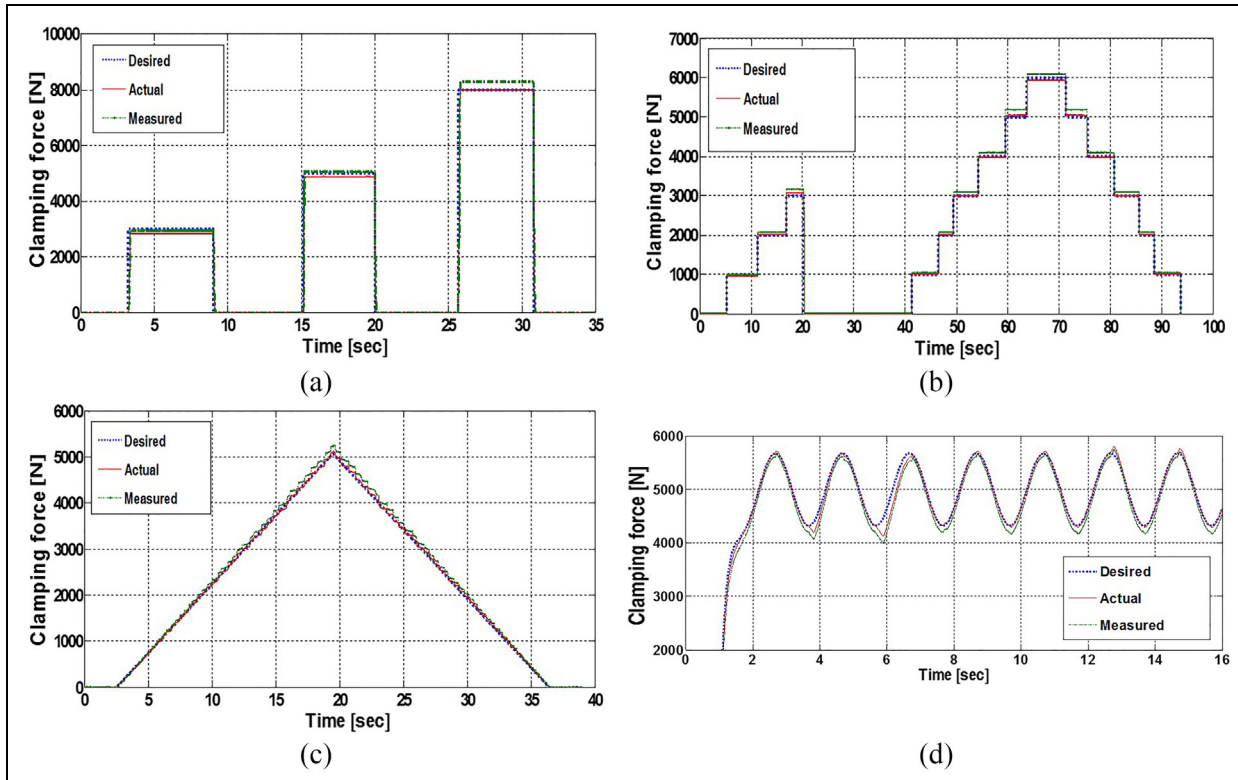


**Figure 9.** Various clamping force commands: (a) step input 1; (b) step input 2; (c) triangular input; (d) sinusoidal input.

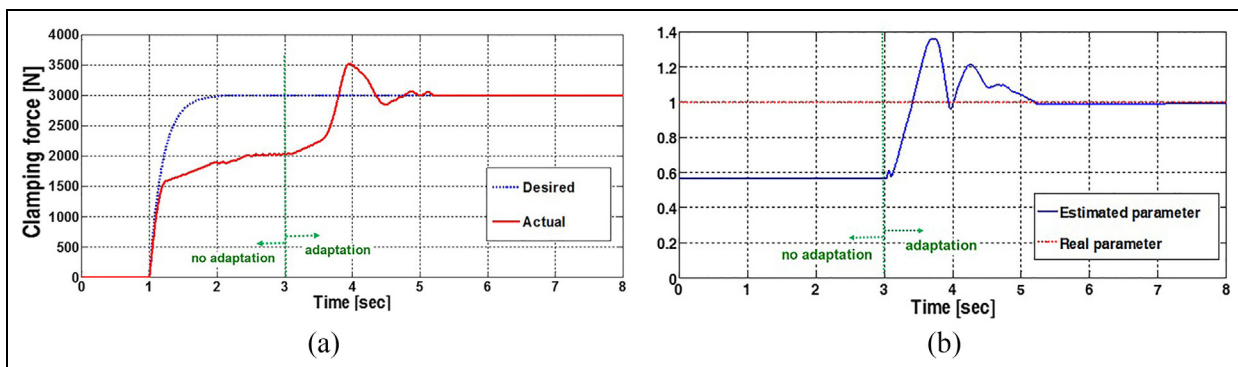


**Figure 10.** Validation of the adaptation law: (a) control results; (b) adaptation of parameter in friction torque.

noticeable amount of overshoot and signal noise are seen. In Figure 12(b), although the steady-state errors between the desired and measured values are seen due to the clamping force estimation error, the root mean square (RMS) error is only 0.27 kN, which is under the error tolerance.

In addition, the control inputs, that is, the motor current values in each controller, are shown in Figure 13. Since the motor current in the existing controller is forced to oscillate largely in order to track the clamping force command, it is distinctly larger than that in the proposed controller. Because the motor current is reduced in the proposed controller, the energy efficiency of the actuator can be improved. Also, the reduced number of tuning parameters of the proposed

controller is beneficial from the viewpoint of tuning simplicity. There is a summary comparison between existing and proposed controllers in Table 4. The controller proposed in this paper shows some advantages: the sensorless system, cost-effective system, less complex gain scheduling, higher energy efficiency, and faster response.

## Conclusion

In this paper, using the readily available motor current and motor angle signals, the clamping force and the friction torque are estimated. The clamping force is expressed as a polynomial with the estimated coefficients. The contact point algorithm plays a major role

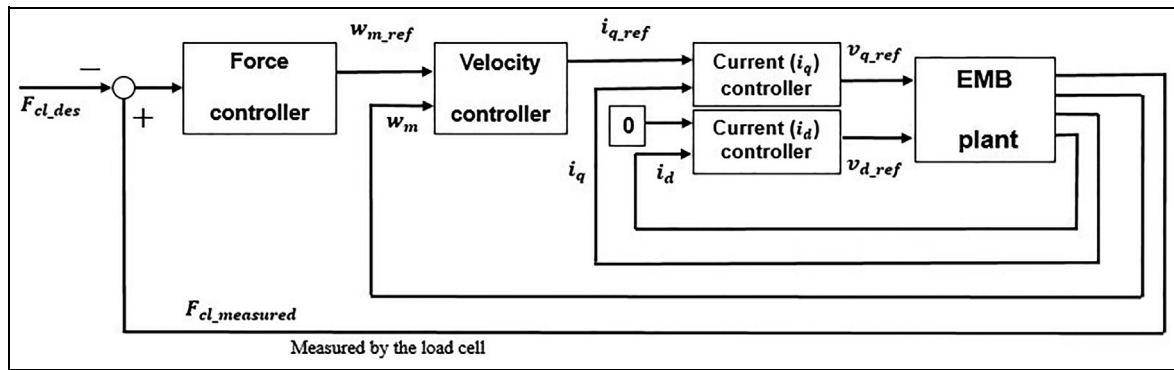


Figure 11. Block diagram of the existing feedback controller. EMB: electromechanical brake.

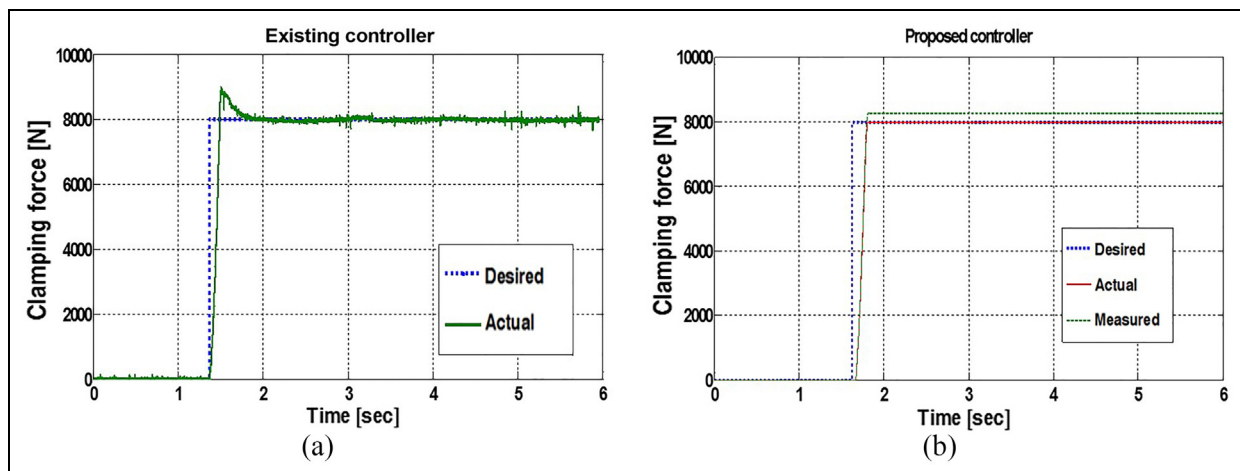


Figure 12. Controller comparison by same step input: (a) existing controller; (b) proposed controller.

Table 4. Comparison between existing and proposed controllers.

Feature	Existing	Proposed
Sensors	Load cell, current sensor, encoder	Current sensor, Encoder
Cost	Too high	Low
Type	Cascaded feedback: force, velocity, current	Adaptive SMC + Feedback (current)
Tuning gains	Three pairs of PI gains	$\lambda, k_d$ , One pair of PI gains
Energy efficiency	Low (large motor current)	High (small motor current)
Transient state	Large overshoot, Long settling time, High tracking performance	Small overshoot, Short settling time, High tracking performance
Steady state	Small error, Noise due to load cell	Acceptable error, No signal noise

PI: proportional–integral; SMC: sliding mode control.

in clamping force estimation. With respect to applicability, these proposed algorithms distinguish themselves from previous estimation algorithms. The lumped friction torque occurring in some components of the EMB is modeled for slipping motion.

Based on the estimation of the dynamic models, a new EMB clamping force controller is proposed. Since

it uses the estimated dynamic models that can be periodically updated and compensated by the adaptive law, it can maintain robustness to changes in parameters. The experimental results of the proposed controller are evaluated and compared to an existing typical feedback controller. Consequently, the proposed controller based on the adaptive SMC method has following



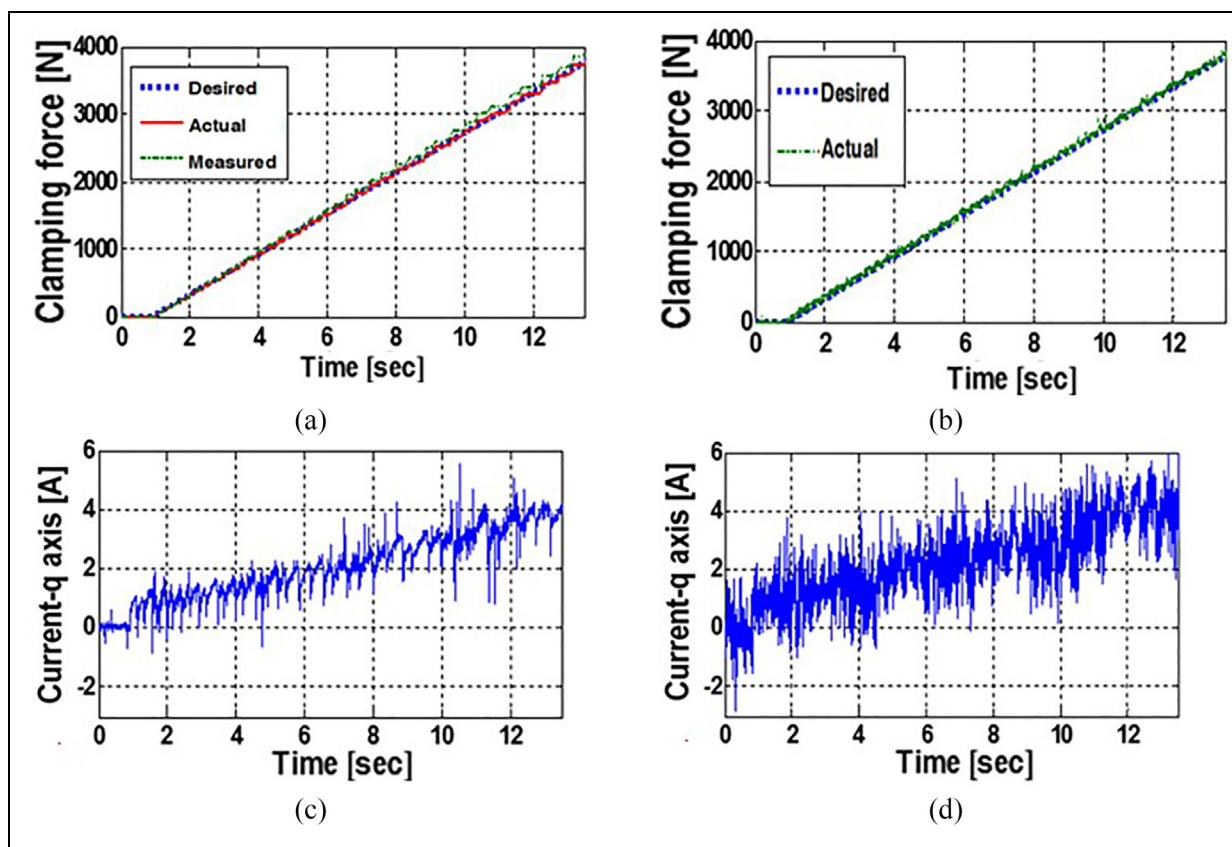


**Figure 13.** Control performance comparison: (a) control results in the proposed controller; (b) control results in the existing controller; (c) motor current in the proposed controller; (d) motor current in the existing controller.

advantages: (a) it is a cost-effective and sensorless algorithm for commercialization of the EMB; (b) due to the reduced number of tuning parameters, it requires less complex gain scheduling than the existing controller; (c) it has higher energy efficiency of the actuator; (d) by using the feed-forward terms, it has a faster response.

This study has demonstrated that the new design of the EMB controller can make a valuable contribution to the development of an outstanding controller for BBWs. As a future work, this controller needs to be combined with the ABS and ESC for vehicle safety.

#### Declaration of conflicting interests

The author(s) declared no potential conflicts of interest with respect to the research, authorship, and/or publication of this article.

#### Funding

The author(s) disclosed receipt of the following financial support for the research, authorship, and/or publication of this article: This work was partly supported by the Hyundai Motor Company; the MSIP (Ministry of Science, ICT and Future Planning), Korea, under the ITRC (Information Technology Research Center) support program (IITP-2017-2012-0-00628) supervised by the IITP (Institute for Information & communications Technology Promotion); the Technological

Innovation R&D program of SMBA (S2341501); the National Research Foundation of Korea (NRF) grant funded by the Korea government (MSIP) (grant number 2017R1A2B4004116); and the BK21+ program through the NRF funded by the Ministry of Education of Korea.

#### References

1. Ki Y, Lee K, Cheon J, et al. Design and implementation of a new clamping force estimator in electro-mechanical brake systems. *Int J Automot Technol* 2013; 14: 739–745.
2. Schwarz R, Isermann R, Bohm J, et al. Modeling and control of an electromechanical disk brake. SAE paper 980600, 1998.
3. Saric S, Bab-Hadiashar A and Hoseinnezhad R. Clamp-force estimation for a brake-by-wire system: a sensor-fusion approach. *IEEE Trans Veh Technol* 2008; 57: 778–786.
4. Hoseinnezhad R and Bab-Hadiashar A. Calibration of resolver sensors in electromechanical braking systems: a modified recursive weighted least-squares approach. *IEEE Trans Ind Electron* 2007; 54: 1052–1060.
5. Jo C, Hwang S and Kim H. Clamping-force control for electromechanical brake. *IEEE Trans Veh Technol* 2010; 59: 3205–3212.
6. Hoseinnezhad R, Bab-Hadiashar A and Rocco T. Real-time clamp force measurement in electromechanical brake calipers. *IEEE Trans Veh Technol* 2008; 57: 770–777.



7. Line C, Manzie C and Good M. Electromechanical brake modeling and control: from PI to MPC. *IEEE Trans Control Syst Technol* 2008; 16: 446–457.
8. Line C, Manzie C and Good M. Control of an electro-mechanical brake for automotive brake-by-wire systems with adapted motion control architecture. SAE paper 012050, 2004.
9. Schwarz R, Isermann R, Bhm J, et al. Clamping force estimation for a brake-by-wire actuator. SAE paper 990482, 1999.
10. Saric S, Bab-Hadiashar A and Walt J. Estimating clamp force for brake-by-wire systems: thermal considerations. *Mechatronics* 2009; 19: 886–895.
11. Allotta B, Pugi L, Paolucci L, et al. Development of sensorless PM servo-system for harsh environments. In: *2015 AEIT international annual conference*, Naples, Italy, 14–16 October 2015. New York: IEEE.
12. Ma S, Zhang T, Liu G, et al. Bond graph-based dynamic model of planetary roller screw mechanism with consideration of axial clearance and friction. *Proc Inst Mech Eng C J Mech Eng Sci* 2017; 0: 1–13.
13. Zhong L, Rahman M, Hu W, et al. Analysis of direct torque control in permanent magnet synchronous motor drives. *IEEE Trans Power Electron* 1997; 12: 528–536.
14. Prokop L, Stulrajter M and Radhostem R. *3-phase PMSM vector control using the PXS20 and tower system*, Roznov pod Radhostem, Czech Republic, TX: Freescale Semiconductor Application Note AN4537, 2012.
15. Pillay P and Krishnan R. Modeling, simulation, and analysis of permanent-magnet motor drives, part I: the permanent-magnet synchronous motor drive. *IEEE Trans Ind Appl* 1989; 25: 265–273.
16. Park H and Choi SB. The development of a sensorless control method for a self-energizing brake system using noncircular gears. *IEEE Trans Control Syst Technol* 2013; 21: 1328–1339.
17. Jo C, Lee S, Song H, et al. Design and control of an upper-wedge-type electronic brake. *Proc IMechE Part D J Autom Eng* 2010; 224: 1393–1405.
18. O'Hem T. *Brake operated shift lock*. Patent 4187935, USA, 1980.
19. Park G, Choi SB and Hyun D. Clamping force estimation based on hysteresis modeling for electro-mechanical brakes. *Int J Automot Technol* 2017; 18: 883–890.
20. Choi M and Choi SB. Linearized recursive least square methods for real-time identification of tire-road friction coefficient. *IEEE Trans Veh Technol* 2013; 62: 2906–2918.
21. Rajamani R. *Vehicle dynamics and control*. New York: Springer, 2006.
22. Karnopp D. Computer simulation of stick-slip friction in mechanical dynamic systems. *J Dyn Sys Meas Control* 1985; 107: 100–103.
23. Olsson H, Astrom K, Wit C, et al. Friction models and friction compensation. *Eur J Control* 1998; 4: 176–195.
24. Chang K, Hedrick J, Zhang W, et al. Automated highway system experiments in the PATH program. *J Intell Transport Syst* 1993; 1: 63–87.
25. Han M, Lee C, Park T, et al. Coupled thermo-mechanical analysis and shape optimization for reducing uneven wear of brake pads. *Int J Automot Technol* 2017; 18: 1027–1035.
26. Ioannou P and Sun J. *Robust adaptive control*. 2nd ed. New Jersey: Prentice-Hall, 1996.
27. Khalil H. *Nonlinear system*. 3rd ed. New Jersey: Prentice-Hall, 2002.
28. Pugi L, Malvezzi M, Tarasconi A, et al. HIL simulation of WSP systems on MI-6 test rig. *Vehicle Syst Dyn* 2006; 44(Suppl. 1): 843–852.

## Appendix

### Notation

$\theta_s, \theta_m$	electrical rotor angle and motor angle
$v_d, v_q$	motor voltages of $d$ -axis/ $q$ -axis
$i_d, i_q$	motor currents of $d$ -axis/ $q$ -axis
$L_d, L_q$	self inductances of $d$ -axis/ $q$ -axis
$\omega_m, \omega_s$	motor/synchronous angular velocities
$R$	stator resistance
$\psi_{af}$	flux linkage
$n_p$	number of pole pairs
$T_m$	motor torque
$K_m$	motor torque constant
$p$	pitch of ball screw
$GR$	gear ratio
$s$	gear efficiency
$x_{screw}$	displacement of ball screw
$k_{screw}$	translating gain of ball screw
$k_{cl}$	gearing gain
$J_{tot}$	total inertia
$F_{cl}$	clamping force
$T_L$	load torque
$T_f$	friction torque
$\gamma$	coefficient of Coulomb friction
$\theta_0$	contact point
$i_0$	threshold of motor current
$i_{q-for}(\theta_m)$	motor current versus motor angle during forward operation
$\alpha_{for}, \beta_{for}$	coefficients of $i_{q-for}(\theta_m)$
$i_{q-back}(\theta_m)$	motor current versus motor angle during backward operation
$\alpha_{back}, \beta_{back}$	coefficients of $i_{q-back}(\theta_m)$
$F_{cl-fitting}(\theta_m)$	characteristic curve
$K_1, K_2$	coefficients of $F_{cl-fitting}(\theta_m)$
$f_1, f_2$	load-dependent coefficients of friction torque
$T_{f0}$	offset term of friction torque